Development and Mechanical Behaviour of Ultra-High Performance Seawater Sea-Sand Concrete

J.G. Teng[1, 2*], Yu Xiang[1], Tao Yu[3] and Zhi Fang[4]

[1]Department of Civil and Environmental Engineering, The Hong Kong Polytechnic University, Hong Kong, China
[2]Department of Ocean Science and Engineering, Southern University of Science and Technology, Shenzhen, Guangdong 518055, China
[3]School of Civil, Mining & Environmental Engineering, University of Wollongong, Wollongong, NSW 2522, Australia
[4]College of Civil Engineering, Hunan University, Changsha, Hunan 410082, China

ABSTRACT

Ultra-high performance concrete (UHPC) is typically defined as an advanced cementitious material that has a compressive strength of over 150 MPa and superior durability. This paper presents the development of a new type of UHPC, namely, ultra-high performance seawater sea-sand concrete (UHPSSC). The development of UHPSSC addresses the challenges associated with the shortage of freshwater, river sand and coarse aggregate in producing concrete for a marine construction project. When used together with corrosion-resistant fibre-reinforced polymer (FRP) composites, the durability of the resulting structures (i.e. hybrid FRP-UHPSSC structures) in a harsh environment can be expected to be outstanding. The ultra-high strength of UHPSSC and the unique characteristics of FRP composites also offer tremendous opportunities for optimization towards new forms of high-performance structures. An experimental study is presented in this paper to demonstrate the concept and feasibility of UHPSSC: UHPSSC samples with a 28-day cube compressive strength of over 180 MPa were successfully produced; the samples were made of seawater and sea-sand, but without steel fibres, and were cured at room temperature. The experimental programme also examined the effects of a number of relevant variables, including the types of sand, mixing water and curing water, among other parameters. The mini-slump spread, compressive strength and stress-strain curve of the specimens were measured to clarify the effects of experimental variables. The test results show that the use of seawater and sea-sand leads to a slight decrease in workability, density and modulus of elasticity; it is also likely to slightly increase the early strength but to slightly decrease the strengths at 7 days and above. Compared with freshwater curing, the seawater curing method results in a slight decrease in elastic modulus and compressive strength.

Keywords: Ultra-high performance concrete; Seawater sea-sand concrete; Seawater; Sea-sand; Concrete mix proportion.

* Corresponding author:
Department of Civil and Environmental Engineering, The Hong Kong Polytechnic University, Hong Kong, China; Department of Ocean Science and Engineering, Southern University of Science and Technology, Shenzhen, Guangdong 518055, China. Email: cejgteng@polyu.edu.hk.

1. INTRODUCTION

Coastal cities rely heavily on their coastal and marine infrastructure (e.g. ports, bridges and offshore wind farms) for social-economic development. The major challenges for coastal and marine infrastructure development include steel corrosion, which is the main cause for infrastructure deterioration, and the shortage of freshwater and river sand for making concrete. To address these challenges, the first author has recently proposed (Teng et al. 2011; Teng 2014) a new type of concrete structures: seawater sea-sand concrete (SSC) structures reinforced with fibre-reinforced polymer (FRP) composites (i.e. FRP-SSC structures). With this new structural concept, seawater and sea-sand can be directly used in constructing coastal and marine infrastructure by capitalizing on the excellent corrosion resistance of FRP composites (Teng et al. 2011; Teng 2014). The idea of SSC structures reinforced with FRP composites has already stimulated a significant amount of recent research (e.g. Li et al. 2016; Wang et al. 2017; Xiao et al. 2017; Li et al. 2018).

Seawater and untreated sea-sand are generally considered to be unsuitable for steel-reinforced concrete structures because of the problem of steel corrosion (BSI 2002; BSI 2013; JGJ 2006; JGJ 2010). Nevertheless, many studies have been conducted on the effects of using seawater instead of freshwater and sea-sand instead of river sand as raw materials for concrete on the properties of concrete, and a review of these studies can be found in Xiao et al. (2017). Compared with freshwater, seawater contains much higher salt contents, represented by the high contents of chloride ions (Cl^-), sulphate ions (SO_4^{2-}), sodium cations (Na^+) and potassium cations (K^+) (Kuche et al. 2015). Compared with river sand, sea-sand contains more salts and coral/seashell particles (Newmon 1968). Coral/seashell particles have a detrimental effect on the workability of concrete and may affect the elastic modulus and strength of concrete (Yang et al. 2005; Richardson et al. 2013). The high concentrations of salt ions in seawater and sea-sand generally lead to a higher early strength (e.g. 7-day strength) but a similar long-term strength of concrete compared with those of conventional concrete made with freshwater and river sand (Kaushik and Islam 1995; Mohammed et al. 2004; Nishida et al. 2013; Etxeberria et al. 2016; Younis et al. 2018); they also lead to a reduced setting time and may affect the workability of concrete (Ghorab et al. 1990; Kaushik and Islam 1995; Younis et al. 2018). Findings from existing studies on the effects of salt ions on the durability of unreinforced concrete are inconclusive: De Weerdt et al. (2014) found that plain concrete is vulnerable to the attack of various salt ions available in seawater, while Otsuki et al. (2014), through a recent survey conducted in Japan, revealed that plain concrete structures made of seawater have very good durability. Nevertheless, it is generally agreed that high-strength SSC has a lower permeability, and is thus more durable, than normal-strength SSC because of the lower water-to-cement ratio of the former (Kaushik and Islam 1995; Otsuki et al. 2014). The existing research on SSC has been limited to SCC with a compressive strength smaller than 80 MPa; no research has been published in the open literature on the use of seawater and sea-sand to make ultra-high performance concrete (UHPC).

UHPC is typically defined as an advanced cementitious material that has a compressive strength of over 150 MPa and superior durability (Richard 1995; Graybeal and Tanesi 2007; Graybeal 2011; Wille et al. 2011; Wille et al. 2014; Wille and Boisvert-Cotulio 2015; Alkaysi et al. 2016). The ultra-high strength of UHPC is generally achieved by increasing its particle packing density, improving the interfacial transition zones between aggregate(s) and the paste matrix, and enhancing its homogeneity (Shi et al. 2015; Wille and Boisvert-Cotulio 2015). Therefore, the production of UHPC normally does not involve the use of coarse aggregate (Shi et al. 2015). To increase the tensile strength and fracture toughness, steel fibres are often used in the mix proportion of UHPC, and such UHPC is also referred to as ultra-high performance fibre-reinforced concrete or UHPFRC (Shi et al. 2015). Steel fibres, although beneficial to the mechanical properties of UHPC, especially its ductility and tensile strength, are expensive and contribute considerably to the high cost of UHPC. Various curing regimes, including room temperature curing, heat curing under atmospheric pressure and autoclave curing, have been used in the production of UHPC, and their effects on the material properties have been investigated. While heat curing and autoclave curing have been found to considerably increase the strength of UHPC (Yazici 2007), they generally involve the use of specific equipment and can be both costly and inconvenient.

The raw materials used to make UHPC typically include water, cement, silica fume, supplemental fine materials [e.g. fly ash, ground granulated blast furnace slag (GGBS), silica powder], high range water reducer (HRWR), aggregate(s) and fibres (Shi et al. 2015; Wille and Boisvert-Cotulio 2015). To enhance the homogeneity of concrete, fine quartz sand with a particle size smaller than 600 μm is commonly used as aggregate in early studies on UHPC (Shi et al. 2015). To reduce the material cost, many researchers have investigated various alternatives to quartz sand (e.g. Yang et al. 2009). These studies have conclusively shown that river sand can be used to replace quartz sand to achieve UHPC with similar properties, if the mix proportion is properly designed (Yang et al. 2009). The particle size of sea-sand is typically between those of quartz sand and river sand, and thus has the potential to be successfully used in producing UHPC.

The water-to-binder ratio of UHPC is typically around 0.2 and is much lower than that of normal strength concrete (e.g. 0.5) (Shi et al. 2015). The permeability of UHPC is low because of its dense microstructure: the chloride diffusion coefficient of UHPC can be as low as 1/55 that of normal strength concrete (Roux et al. 1996). Therefore, the detrimental effects of salt ions from both the mixing water and the water from the environment can be expected to be much smaller for UHPC than for normal strength concrete. There is thus a great potential for UHPC to be made of seawater and to be used in coastal and marine environments.

Against the above background, this paper presents the first ever experimental study on the development of UHPC with seawater and sea-sand (i.e. ultra-high performance seawater sea-sand concrete or UHPSSC). In the present study, the UHPSSC was made without steel fibres to reduce costs and eliminate steel corrosion concerns, and was cured at room temperature. The absence of steel fibres means that the present UHPSSC, in strict terms of conventional terminology, is a plain UHPSSC or a UHPSSC matrix. In practical applications, the potential weaknesses associated with the elimination of steel fibres can be addressed at material level by incorporating non-metallic fibres, or at component level by the combined use of the present UHPSSC with FRP confinement. For example, the present UHPSSC can be used with filament-wound FRP tubes to form hybrid columns, in which the ductility of UHPSSC in compression can be greatly enhanced by FRP confinement. Teng et al. (2018) has recently proposed a novel type of steel-free reinforcing bars (referred to as hybrid bars) for use in seawater sea-sand concrete, and such a hybrid bar typically consists of an FRP tube filled with plain UHPSSC which is centrally reinforced with an FRP bar. In these hybrid bars, the UHPSSC can be well confined by the FRP tube, so the absence of steel fibres from the UHPSSC does not create any concerns.

2. EXPERIMENTAL PROGRAMME

2.1 Mix design

In the present study, 15 different mixes were prepared and tested. The mixes all had the same proportions of the six constituents [i.e. cement, silica fume (SF), supplemental fine materials (SM), fine aggregate, water and HRWR]; the main differences between the mixes were the raw materials used. The mix proportions were developed by a trial-and-error process based on the recommendations provided by Wille and Boisvert-Cotulio (2015).

Mixes 1 to 5 were designed to investigate the effect of salinity of mixing water and are referred to collectively as Group 1. The five mixes were all prepared with quartz sand (QS) and the so-called artificial seawater (ASW), which was made of tap water (TW) and dissolved commercial sea salt of various doses. Mixes 6 to 10 (referred to collectively as Group 2) were all prepared with river sand (RS) and tap (fresh) water, while Mixes 11 to 15 (referred to collectively as Group 3) were all prepared with sea-sand (SS) and natural seawater (SW). Other than that, Groups 2 and 3, each with 5 mixes, were both so designed that the effects of a different cement [i.e. white cement (WC) or ordinary Portland cement (OPC)] and a different supplemental material [i.e. quartz powder (QP) or Class C fly ash (FA)], as well as the effect of sand washing, can be investigated. Table 1 summarizes the details of all the 15 mixes.

Each mix is given a name, which consists of four components representing the fine aggregate, water, cement and supplemental material used in the mix, respectively. In the present study, the river sand and sea-sand were washed before being used, except for Mixes 6 and 11 in which untreated river sand (uRS) and untreated sea-sand (uSS) were used. Therefore, in the mix names, "RS" and "SS" were used only for treated river sand and treated sea-sand, respectively. For example, the name SS-SW-WC-QP represents a mix with treated sea-sand, natural seawater, white cement and quartz powder.

2.2 Raw Materials

2.2.1 Cement

Existing research (e.g. Sakai et al. 2008; Graybeal 2011; Wille and Boisvert-Cotulio 2015) suggests that white cement, which is rich in the sum of C_3S and C_2S, is preferred in making UHPC to ensure favorable strength development and workability. White cement, however, is considerably more expensive than ordinary Portland cement. In the present study, an EN 197-1 CEM I 52.5N white cement and an EN 197-1 CEM I 52.5N ordinary Portland cement, both produced by the Green Island Cement (Holdings) Limited, Hong Kong, were used to clarify their effects on concrete properties.

The chemical compositions of the two cements, analysed by X-ray fluorescence (XRF) spectroscopy (AXS GmbH, Bruker), are summarized in Table 2, in which the Bogue components were calculated based on the Bogue equations (Hewlett 1998). Compared with the ordinary Portland cement, the white cement was found to have high contents of C_3S and C_2S. In addition, the Fe_2O_3 content in the white cement (i.e. 0.41%) was very low compared with that in the ordinary

Portland cement (i.e. 3.04%), which is the main reason for its white color (Hamad 1995). The specific surface area of the white cement (3540 cm^2/g) was found to be smaller than that of the ordinary Portland cement (3840 cm^2/g).

2.2.2 Silica Fume and Supplemental Materials

The silica fume used in all mixes were produced by Sap Corp., China. The chemical composition of the silica fume is given in Table 2, which shows that it had a silica content of over 94%.

Two supplemental materials were used in the present study: quartz powder with a mean particle diameter of 7.47 μm from the Y.S. Corp., China, and fly ash with a mean particle diameter of 8.96 μm produced by CLP Power Ltd., Hong Kong. The quartz powder had a silica content of over 96%, while the fly ash had a sum of oxides (SiO_2+Al_2O_3+Fe_2O_3) in the range of 50% to 70% and can thus be classified into a Class C fly ash according to ASTM C618 (2017) (Table 2).

Quartz powder has often been used in making UHPC because of its high material purity (Wille and Boisvert-Cotulio 2015). However, the use of fly ash is more environmentally friendly and economical. In addition, the spherical particle shape and pozzolanic reactivity of fly ash have been reported to benefit the workability, the long-term strength development and the durability of concrete (Hemalatha and Ramaswamy 2017).

2.2.3 Water

Local tap water in Hong Kong was used as freshwater in the present study. The chemical composition of the tap water, measured from ion chromatography (IC) tests, is given in Table 3. It is evident from Table 3 that the salinity of the tap water was very small (<0.1 g/L).

Two sources of mixing water were often used in existing studies on seawater concrete: natural seawater and artificial seawater made of tap water and dissolved commercial sea salt. In the present study, natural seawater was used in Mixes 11-15, while artificial seawater was used in Mixes 2-5 so that the salinity of mixing water could be precisely controlled to investigate its effects.

Natural seawater was obtained from three locations along the coast of Hong Kong, and their chemical compositions were measured and compared with the world-average composition in Table 3. It is evident that the chemical compositions of seawater from the three sources are all close to the world-average composition. The seawater from Chek Lap Kok (CLK), which is away from residential areas, was used in Mixes 11-15 of the present study.

To select the most suitable salt for making artificial seawater, three commercial sea salts were dissolved in tap water respectively, all with a dose of 36 g/L, and the chemical compositions of the three types of resulting artificial seawater were measured. Table 3 shows that the Cl^- content in Artificial Seawater 1 is slightly lower than the world-average value, but the contents of other ions (e.g. Br^-, SO_4^{2-}, NO_3^-, Mg^{2+} and Ca^{2+}) in Artificial Seawater 1 are much closer to the corresponding world-average values of natural seawater than those in Artificial Seawater 2 and 3. Therefore, Sea Salt 1 was used in the present study (i.e. for Mixes 2-5) for making artificial seawater. The doses of sea salt for making the artificial seawater used in Mixes 2-5 are 18 g/L, 36 g/L, 54 g/L and 72 g/L, respectively, representing around 50%, 100%, 150% and 200% of the salinity of typical natural seawater. The artificial seawater is thus denoted by 50ASW, 100ASW, 150ASW, 200ASW in the names of Mixes 2-5, respectively.

2.2.4 Sand

The sea-sand used in the present study was mined from CLK, Hong Kong, which is consistent with the source of the natural seawater. The quartz sand was from the Y.S. Corp., China, while the river sand was purchased from the local market in Hong Kong. Particles with a size of larger than 1.18 mm were eliminated from the sands before being used as suggested by Wille and Boisvert-Cotulio (2015).

Existing research (Fernandes et al. 2007) suggests that the high content of clay in original river sand and sea-sand may have detrimental effects on the workability and strength of UHPC. Therefore, for most mixes in the present study, the river sand or the sea-sand were washed with tap water to eliminate the clay. Unwashed river sand and unwashed sea-sand were only used for comparison in Mixes 6 and 11, respectively. It should be noted that sea-sand should ideally be washed by seawater, which is expected to be the case in practice, instead of tap water which may change the salt concentration of sea and. Tap water was used for washing sea-sand in the present study because of the difficulty of obtaining a large amount of natural seawater. Nevertheless, to minimize the potential effects, the washed sea-sand was soaked in natural seawater for 48 hours after being washed. After the above desilting process, the river sand or sea-sand was dried at 105°C for 48 hours and then stored until being used. In accordance with GB/T (2011), the silt contents of sea-sand and river sand before desilting were measured to be 5.46% and 0.61%, respectively, while the values for desilted sea and river sands were 1.54% and 0.25%, respectively.

IC tests were conducted to obtain the chemical compositions of the lixiviums of four kinds of sands: original (unwashed) river sand and sea-sand, as well as washed sea-sand before and after being soaked in seawater for 48 hours. The results summarized in Table 4 show that the original river sand had a salinity (0.3579 g/L) much lower than that of the original sea-sand (i.e. 4.6809 g/L), and contained a very small Cl content (i.e. 0.0119 g/L). It is also evident that after being washed by tap water, the salinity of sea-sand was dramatically reduced, but it then returned to a level close to that of the original sea-sand after being soaked in seawater for 48 hours.

The particle size distributions (PSD) of the sands used in the mixes are shown in Figure 1. It is evident that the desilting process had little effect on the PSD. It is also evident that compared to the river sand, the sea-sand contained more fine particles (e.g. those with a size between 0 to 300 μm) (Figure 1). The shell contents of desilted sea and river sands were measured to be 1.19% and 0.87%, respectively, in accordance with JGJ 52 (2006). These values are lower than those typically reported by previous researchers (e.g. 4.4% for sea-sand as reported by Liu et al. 2016), which is believed to be at least partially due to the elimination of particles larger than 1.18 mm in the present study.

2.2.5 HRWR

A polycarboxylate-based superplasticizer produced by the BASF chemical company, Hong Kong, was used as the HRWR in the present study. The superplasticizer had a solid content of 22% by mass and a specific gravity of 1.05.

2.3 Methodology

2.3.1 Mixing, Casting and Curing Methods

The preparation process of UHPC included two steps: (1) mixing dry constituents (i.e. cement, silica fume, supplemental material and sand) for 5 minutes; (2) mixing water with HRWR and adding the mixture in two steps, and then mixing for another 8 minutes until the UHPC reached an acceptable level of fluidity.

The freshly mixed UHPC was slowly filled into 50 mm cube moulds and *Φ*75 mm × 150 mm cylinder moulds, and then vibrated on a vibration table for 2 minutes to eliminate air voids in the concrete. After casting, all moulds were covered with a plastic sheet within 10 minutes. All specimens were demoulded after 24 hours.

Three kinds of curing methods were adopted in the present study after demoulding: (1) tap water curing: 15 cube samples and 3 cylinder samples of each mix were immersed in tap water at 22±3°C using a thermostatic water tank until the specific ages for testing; (2) seawater curing: 15 cube samples and 3 cylinder samples of Mixes 12 and 13 were immersed in seawater at 22±3°C using another thermostatic water tank until specific ages for testing; and (3) 24-hour heat curing: 3 cube samples of each mix were immersed in a programmable accelerated curing tank with hot tap water at 90±1°C for 24 hours.

2.3.2 Workability

In previous studies (Wille et al. 2011; Wille and Boisvert-Cotulio 2015; Meng and Khayat, 2017; Soliman and Tagnit-Hamou 2017), a dynamic mini-slump spread was usually measured in accordance with ASTM C1473 (2015) using a flow table specified in ASTM C230 (2014). However, trial tests using the above method showed that the slump spreads of UHPC/UHPSSC in the present study exceeded the maximum diameter of the flow table (i.e. 255±2.5 mm) after 25 drops within 15 seconds. The observation suggested that accurate slump spreads cannot be obtained using this method. Therefore, a free mini-slump spread test was performed in accordance with ASTM C1856 (2017) to determine the workability of UHPC/UHPSSC in the present study.

2.3.3 Density

The densities of all specimens at ages of 1, 28 and 90 days were obtained in accordance with ASTM C642-13 (2013), in which the following equation is given for the calculation of hardened density of a specimen:

$$\rho = \frac{W_{\mathrm{a}}}{W_{\mathrm{a}} - W_{\mathrm{w}}} \times \rho_{\mathrm{w}} \quad (1)$$

where W_a is the weight of a specimen measured in air; W_w is the weight of a specimen measured in water; ρ_w is the density of water and ρ_w =1000 kg/m^3.

2.3.4 Cube Compressive Strength

Standard concrete cube tests (50 mm) were conducted to obtain the compressive strengths at ages of 1, 7, 14, 28 and 90 days in accordance with ASTM C109 (2016). For each age of each mix, three specimens were tested, and the average value was obtained. The loading rate of 1 MPa/s was adopted so that each test was completed around three minutes.

2.3.5 Compressive Stress-Strain Relationship

Standard concrete cylinder tests (Φ75 mm × 150 mm) were conducted at an age of 35 days to obtain the compressive stress-strain relationship in accordance with ASTM C1856 (2017). An MTS testing system was used for these tests with a displacement control rate of 0.18 mm/min, which is similar to the loading rate of 1 MPa/s used for the initial stage of loading. A total of six strain gauges, three in the axial direction with a gauge length of 50 mm and another three in the hoop direction with a gauge length of 30 mm, were installed on each specimen. Figure 2 shows the test setup and layout of strain gauges.

2.3.6 Material Supplies

Only a single supply of each raw material for the concrete was used during the present experimental program to ensure the consistency of material quality and properties.

3. EXPERIMENTAL RESULTS AND DISCUSSIONS

3.1 Workability

The workability of UHPC is associated with the good packing of raw constituent materials as well as the compatibility of cementitious materials with the HRWR (Meng and Khayat 2017), and is normally checked using various slump tests. The slump spreads obtained from free mini-slump spread tests are summarized in Table 5 for all the 15 mixes of the present study.

The results of Group 1 (Mixes 1-5) show that the workability of UHPC generally decreases with the salinity of mixing water (Table 5). The slump spread of Mix 5 using artificial seawater with a salinity of 72 g/L was only around 50% of that of Mix 1 using tap water. This is believed to be at least partially due to the existence of $CaCl_2$ in the artificial seawater, which accelerated the formation of C-S-H and heat release in the hydration process (Juengera et al. 2016).

A comparison between the results of Group 2 (Mixes 6-10) and Group 3 (Mixes 11-15) shows that the use of seawater and sea-sand generally leads to decreases in the slump spread, and the degree of decrease appears to be also dependent on other raw constituent materials used in the mix. This observation is consistent with findings from previous studies (Mohammed et al. 2004; Kaushik and Islam 1995; Islam et al. 2012). Besides the accelerated hydration due to the existence of salts, it is believed that the finer particles (and thus larger surface areas) of sea-sand, as compared with river sand, may also contribute to this decrease in workability (Hasdemir et al. 2016).

A comparison between the five mixes (Mixes 6-10) of Group 2 shows evidently the effects of various raw constituent materials. The desilting of sand and the replacement of quartz powder with fly ash led to increases in the slump spread, while the replacement of white cement with ordinary Portland cement was found to negatively affect workability. These observations are consistent with previous studies on UHPC and are believed to be at least partially due to the fineness (or surface areas) of the raw constituent materials: the desilting of sand reduced significantly its amount of clay which consists of very fine particles (Fernandes et al. 2007), while compared with the white cement, the ordinary Portland cement used in the present study had a larger specific surface area. In addition, compared with the quartz powder, the fly ash has the potential of pozzolanic reactions and may reduce frictions between aggregate particles because of its spherical shape of particles, which both contribute to increased slump spreads (Hemalatha and Ramaswamy 2017).

Similar observations can be made when comparing the five mixes (Mixes 11-15) of Group 3, which were prepared with seawater and sea-sand. The only notable difference is that the effect of desilting process seems to be much more pronounced for sea-sand than for river sand, probably due to the larger content of clay in the former (i.e. 5.46%) compared to that in the latter (i.e. 0.61%).

3.2 Density

The densities of UHPC at different ages are summarized in Table 5 for all the 15 mixes. These results were obtained using samples subjected to tap water curing at room temperature (i.e. tap water curing). In the subsequent sections, unless otherwise specified, the reported test results were all obtained from samples subjected to tap water curing.

In general, the density increases with the age for all the mixes because of the continuous water absorption process of the concrete when immersed in water (Table 5). The effects of various parameters of the mix on the density appear to be similar to those on the workability: the density generally decreases with the salinity for the five mixes (Mixes 1-5) of Group 1, while the use of seawater and sea-sand generally led to a decrease in density (see results of Groups 2 and 3). The density is shown against the slump spread in Figure 3 to further examine the correlation between the two. It is evident that they are almost linearly correlated (Figure 3).

3.3 Cube Compressive Strength

Table 6 summarizes the results of cube compressive strengths of all mixes at different ages. In Table 6, the mean value and the standard deviation (SD) were both obtained based on the results of three nominally identical specimens. It is evident from Table 6 that the UHPSSC made in the present study reached a 28-day cube compressive strength of up to 184 MPa.

The results of specimens with Mixes 1-5 of Group 1 are compared in Figure 4 to examine the effect of salinity of mixing water on the compressive strength of concrete. For ease of comparison, the compressive strengths of different mixes are also normalized with the corresponding strength of Mix 1 at the same age in Figure 4 (referred to as normalized f_{cu}). It is evident from Figure 5 that:

(1) the 7-day strengths of Mixes 2-5 are generally higher than that of Mix 1, suggesting that the use of saltwater generally leads to a higher early strength of concrete; (2) the strengths of Mix 2 with a salinity of 18 g/L at various ages are all higher than Mixes 1 and 3-5, suggesting that an optimum salinity of mixing water, equal or close to that of Mix 2, may exist for the compressive strength of concrete; (3) the 14-day, 28-day and 90-day strengths of Mixes 3-5 are slightly lower than Mix 1, and appear to decrease with an increase in salinity, suggesting that when the salinity of mixing water exceeds a certain value, it may have a slight negative effect on the long-term compressive strength of concrete. Similar observations were also made in existing studies on normal strength concrete mixed with saltwater (e.g. Taylor and Kuwairi 1978; Kaushik and Islam 1995; Tiwari et al. 2014). It is believed that the slightly higher early strength of concrete with saltwater is due to the formation of the so-called Friedel's salt ($3CaO{\cdot}Al_2O_3{\cdot}CaCl_2{\cdot}10H_2O$) and Kuzel's salt ($3CaO{\cdot}Al_2O_3{\cdot}0.5CaSO_4{\cdot}0.5CaCl_2{\cdot}11H_2O$) because of the existence of chloride ions (Weerdt et al 2014); the decomposition of these salts with time, on the other hand, is believed to affect the long-term strength of concrete (Suryavanshi and Swamy 1996).

Figure 5 compares the results of Groups 2 and 3. In Figure 5, the only difference between the two mixes in each subfigure is that one mix (of Group 2) used river sand and tap water while the other (of Group 3) used sea-sand and seawater. The results indicate that due to the use of sweater and sea-sand, the early strength is likely to increase, but the strengths at 7 days and above are likely to decrease, although these trends are not shared by one of the sub-figures. Nevertheless, the differences at various ages between the two mixes in each of the four subfigures are all within 8% except for the 1-day strength of one pair (Figure 5d), suggesting that the use of seawater and sea-sand to replace tap water and river sand only has a small effect on the compressive strength of UHPC. This observation is also consistent with previous research on normal strength concrete, which reported that chloride ion-induced strength variations are generally within 10% (Younis et al. 2018; Kaushik and Islam 1995).

The effect of using Class C fly ash to replace quartz powder is illustrated in Figure 6 by comparing four pairs of mixes; the only difference between the two mixes in each pair is the supplemental fine material (i.e. fly ash or quartz powder). It is evident that the mixes with fly ash have similar strengths to those of the mixes with quartz powder at an age of 7 days or above. The variation in 1-day strength in Figure 6d may be attributed to the scatter of test data of Mix 14 in Group 3 (i.e. SS-SW-OPC-QP). Fly ash is known to have the potential of pozzolanic reactions (Papadakis 2000; Hemalatha and Ramaswamy 2017) which may be beneficial to the strength development of concrete, but the high content of free calcium oxide (i.e. CaO) of Class C fly ash may negatively affect the concrete strength especially with the presence of sulphate ions (Tikalsky and Carrasquillo 1989). The observation illustrated in Figure 6 is believed to be a result of counteracting effects of many factors, including the two mentioned above. Further research involving analysis of the material structure of UHPSSC is needed to clarify these effects.

Figure 7 illustrates the effects of cement type; the only difference between the two mixes in each subfigure of Figure 7 is the type of cement (i.e. white cement or ordinary Portland cement). It is evident that the use of ordinary Portland cement to replace white cement generally leads to lower early age strengths, especially the 1-day strength, but its effect on the 28-day and 90-day strengths seems dependent on other constituents of the mix: for Group 2 with river sand and tap water, the mixes with ordinary Portland cement have higher 28-day and 90-day strengths, but the opposite was found for Group 3 with seawater and sea-sand.

Figure 8 shows the effect of sand desilting on the concrete strength. It is evident that the mixes with washed sand generally have higher strengths at various ages compared with their counterparts with unwashed sand. This effect appears to be more pronounced for the sea-sand group (Figure 8b) due to the relatively high clay content in the unwashed sea-sand: sand desilting is shown to lead to an increase of around 10% in the 28-day strength of this group. This is not a surprise as the negative effect of clay in sand (e.g. weakening the bond between sand and cement paste) has been well recognized by existing research (e.g. Fernandes et al. 2007).

Previous research (e.g. Wille et al. 2011; Wille and Boisvert-Cotulio 2015) has shown that the compressive strength of UHPC has a strong correlation to its rheological properties (e.g. slump spread), as the latter is an indicator of its particle packing density. The 28-day cube compressive strengths ($f_{cu,28d}$) of all mixes are shown against their respective slump spreads (D) in Figure 9, which reveals clearly the correlation between the two for all the mixes including those prepared with seawater and sea-sand.

3.4 Compressive Stress-Strain Relationship

Figure 10 shows the compressive stress-strain curves obtained from standard cylinder tests for nine mixes of Groups 2 and 3. The axial strain and hoop strain values shown in Figure 10 were both averaged from the readings of three strain gauges. It should be noted that since Specimen 2 of Mix 13 and Specimen 3 of Mix 14 failed prematurely due to operational errors during the pre-loading process, only results for the remaining two specimens for each of the two mixes (i.e. Mixer 13 and 14) are presented in Figures 10g and 10h respectively. Similar to the observations reported in the open literature (e.g. Wu et al. 2016), the stress-strain curves all have an almost linear shape as no fibres were used in the mixes. All test cylinders failed in a brittle manner and thus the descending branch of the stress-strain curves could not be captured during the tests.

The characteristic parameters of the stress-strain curves are summarized in Table 7, in which the cylinder compressive strength (f_{co}) as well as the corresponding axial (ε_{co}) and hoop strains (ε_{lo}) were the stress and strain values at the peak point on the curve, while the modulus of elasticity (E_c) and the Poisson's ratio (υ) were calculated in accordance with ASTM C469 (2014).

The elastic modulus and the axial and hoop strains at the peak stress are shown against the cylinder compressive strength in Figures 11a-11c, respectively. Figure 11a shows that the elastic moduli of specimens in Group 2 are slightly larger than those of the corresponding UHPSSC specimens in Group 3 with the same compressive strength, suggesting that the use of seawater and sea-sand may have a slight negative effect on the value of elastic modulus. By looking at all the data points in Figure 11b and 11c, it appears that the axial and hoop strains at the peak stress of specimens in Group 2 are both slightly smaller than those of the corresponding UHPSSC in Group 3 with the same compressive strength. The above observations are further evidenced by the two trend lines in each of the subfigures, which were obtained from linear regression analyses for the two groups, respectively. In addition, the measured axial strain at peak stress ranges between 3870 με and 4473 με. These values are larger than that of normal high-strength concrete with a compressive strength of less than 100 MPa (Carreia and Chu 1985; Lu and Zhao 2010), but they are consistent with those reported in the existing research on UHPC (Sobuz et al. 2016; Hoang and Fehling 2017). The Poisson's ratios (υ) of all the mixes, however, are consistently 0.20 or 0.21, despite the variations in raw constituent materials and compressive strength.

The average cylinder compressive strengths of the nine mixes are shown against their cube compressive strengths in Figure 12, which show that the former is slightly larger for the same mix. This is opposite to the common observation for normal strength concrete, but is consistent with the findings by Kusumawardaningsih et al. (2015) for UHPC. However, even for UHPC, Graybeal and Davis (2008) found that the cylinder compressive strength is lower than the cube compressive strength. In the present study, the end surfaces of the cylinder specimens were ground to ensure that they were flat and parallel, but the surfaces of the cube specimens, which satisfied the requirement of the standard (ASTM C109 2016), were not ground. In addition, although the cylinder specimens were prepared using exactly the same mix proportions as the cube specimens, they were prepared in different batches. The above two factors might also have affected the test results. Further research is needed to clarify the relationship between the cube and cylinder compressive strengths of UHPC.

3.5 Effect of Curing Method

Figure 13 compares the results of two pairs of specimens; the only difference between the specimens in each pair was the curing method. It is evident that compared with tap water curing, seawater curing led to evident reductions in the compressive strength of concrete (up to around 15% at the age of 90 days), and such a reduction appears to increase with the age of concrete. The seawater curing method also appears to have a slight negative effect on the elastic modulus of concrete, but this effect was not as pronounced as the effect on strength (see Table 8). The above observations are similar to those reported in the open literature (e.g. Etxeberria et al. 2016; Islam et al. 2016), and are believed to be at least partially due to the existence of magnesium sulphate when seawater is used for curing (Ragab et al. 2016).

In Figure 14 the compressive strengths of specimens after 28 and 90 days of 22±3°C tap water immersion curing (i.e. $f_{cu,28d}$ and $f_{cu,90d}$) are shown against the strengths of the corresponding specimens after 24 hours of 90±1°C heat curing (i.e. $f_{cu,H\text{-}24hr}$). Trend lines obtained using linear regression analyses are also given in the figure to show the correlation between results obtained with different curing methods. In addition, the $f_{cu,H\text{-}24hr}$ values of all the mixes are summarized in Table 6. It is evident from Figure 14a and Table 6 that $f_{cu,H\text{-}24hr}$ is generally close to $f_{cu,28d}$ while lower than $f_{cu,90d}$ for the mixes of Group 2. However, for the UHPSSC mixes of Group 3, Figure 14b shows that both $f_{cu,28d}$ and $f_{cu,90d}$ are lower than $f_{cu,H\text{-}24hr}$. It may thus be concluded that compared with UHPC, it takes more time for UHPSSC cured at room temperature to develop the same strength as that subjected to heat curing.

4. COST ANALYSIS

The cost per cubic meter within the Hong Kong context was calculated for the mixes in Group 3 (i.e. UHPSSC) and compared with that of normal concrete having a cylinder compressive strength of 54.1 MPa, whose mix proportions are given in Zhang et al. (2014). In the calculations, the following prices of the raw materials, obtained in July 2018 from the suppliers of materials used in the present study, were used: (1) HKD 2080 per tonne for white cement; (2) HKD 810 per tonne for ordinary Portland cement; (3) HKD 2070 per tonne for silica fume; (4) HKD 2300 per tonne for quartz powder; (5) HKD 300 per tonne for fly ash; (6) HKD 750 per tonne for quartz sand; and (7) HKD 13000 per tonne for HRWR. The prices of natural river sand and crushed stone are assumed to be HKD 138 per tonne and HKD 67 per tonne, respectively, according to the Census and Statistics Department (CSD) of Hong Kong (HK CSD 2018a). Natural sea-sand is abundant in coastal regions, so it may be used at no cost. However, in the calculations, it is conservatively assumed to cost the same amount as river sand (i.e. HKD 138 per tonne). Similarly, seawater is conservatively assumed to have the same cost of HKD 7.11 per tonne as tap water according to the Water Supplies Department (WSD) of Hong Kong (HK WSD 2018).

The desilting of sand was found to increase the compressive strength of UHPSSC. The desilting process involves additional energy and labour costs, which are estimated to be HKD 2.05 per tonne based on the following assumption: (1) a typical 15 kW sand washing machine (e.g. Model KSW 200) (Mewarhitech 2018) capable of washing 130 tonnes of sand per hour; (2) the cost for electricity is HKD 1.15 per kWh (CLP 2018); and (3) two workers are needed to operate such a sand washing machine and their average salary is HKD 998.2 per day (HD CSD 2018b). The labour and equipment costs for casting concrete are negligible compared with other costs, so they are not included in the calculations for simplicity.

The so-calculated costs per cubic meter are summarized in Table 9. It is evident that significant reductions in the costs can result from the use of ordinary Portland cement to replace white cement, and the use of fly ash to replace quartz powder. The cost per unit volume of UHPSSC is shown to be significantly higher than that of normal concrete. However, considering its ultrahigh strength, the cost per MPa per cubic meter of UHPSSC is comparable to or even lower than that of normal concrete. The UHPSSC mix with ordinary Portland cement and fly ash (i.e. SS-SW-OPC-FA) is the most cost-effective, with a cost of only HKD 9.43 per MPa per cubic meter.

In the above calculations, seawater and sea-sand were assumed to cost the same amounts as tap water and river sand, respectively. By doing so, the costs per cubic meter of Mixes 11-15 (UHPSSC) are exactly the same as those of Mixes 6-10 (tap water-river sand UHPC), respectively. In practice, seawater and sea-sand may be obtained at nearly no cost so that the costs of UHPSSC can be further reduced to the numbers provided in the brackets of Table 9.

5. CONCLUSIONS

This paper has been concerned with the development of ultra-high performance concrete using seawater and sea-sand (referred to as UHPSSC) to address the challenges associated with the shortage of fresh water, river sand and coarse aggregate in producing concrete for coastal and marine infrastructure. To minimise the cost of producing UHPSSC and eliminating corrosion concerns with steel fibres, the study has been focussed on the development and behaviour of UHPSSC without short steel fibres. The paper has presented an experimental study to demonstrate the concept of UHPSSC and to clarify the effects of several parameters on its mechanical behaviour. The test results showed that the highest-strength UHPSSC in the present study, which was prepared with white cement, silica fume and quartz powder and cured at room temperature, achieved a 28-day cube compressive strength of 184 MPa, with its mini-slump spread, modulus of elasticity and Poisson's ratio being 324 mm, 51 GPa and 0.21, respectively. The results and discussions presented in the paper also allow the following conclusions to be drawn:

(1) The use of seawater and sea-sand generally leads to decreases in the workability and the density of UHPC. Such decreases are shown to be dependent on the other constituent materials and can be small.
(2) The use of seawater and sea-sand is likely to slightly increase the early strength of UHPC but is likely to slightly decrease the strengths at 7 days and above.
(3) Compared to tap water-river sand UHPC, the UHPSSC with the same compressive strength generally has a slightly lower modulus of elasticity but slightly higher axial and hoop strains at peak axial stress.
(4) Sand desilting results in a considerable increase in the workability and strength of UHPSSC. The use of ordinary Portland cement to replace white cement leads to a slight decrease in the workability and early strength of UHPSSC, whereas the use of Class C fly ash to replace quartz powder leads to a slight increase in the workability of UHPSSC.
(5) The cost per MPa per cubic metre of UHPSSC is comparable to or even lower than that of a normal concrete with a cylinder compressive strength of 54.1 MPa. The most cost-effective UHPSSC in the present study, which was mixed with ordinary Portland cement and Class C fly ash, has a unit cost of only HKD 9.43 per MPa per cubic meter and a 28-day cube compressive strength of 174 MPa.

ACKNOWLEDGEMENTS

The authors gratefully acknowledge the financial support provided by the Hong Kong Research Grants Council (Project Nos: PolyU 152634/16E and T22-502/18-R) and The Hong Kong Polyethnic University (Project account code: 1-BBAG). The authors would also like to thank Messrs Ze-Jian Chen, Ryan Ho and Jia-Chen Ma for their assistance in the execution of the tests and BASF Chemical, Hong Kong for donating the HRWR used in the tests. They would also like to thank Drs Lik Lam, Cheng Jiang, Botong Zheng and Rui Zhong for helpful discussions during the study.

REFERENCES

ASTM. (2016). Standard test method for compressive strength of hydraulic cement mortars (using 2-in. or [50-mm] cube specimens). *ASTM C109/C109M-16a*, West Conshohocken, PA.
ASTM. (2014). Standard specification for flow table for use in tests of hydraulic cement. *ASTM C230/C230M - 14*, West Conshohocken, PA.
ASTM. (2014). Standard test method for static modulus of elasticity and poisson's ratio of concrete in compression. *ASTM C469/C469M-14*, West Conshohocken, PA.
ASTM. (2017). Standard specification for coal fly ash and raw or calcined natural pozzolan for use in concrete. *ASTM C618 - 17a*, West Conshohocken, PA.
ASTM. (2013). Standard test method for density, absorption, and voids in hardened concrete. *ASTM C642 - 13*, West Conshohocken, PA.
ASTM. (2015). Standard test method for flow of hydraulic cement mortar. *ASTM C1437/C1437M-15*, West Conshohocken, PA.

ASTM. (2017). Standard practice for fabricating and testing specimens of ultra-high performance concrete. *ASTM C1856/C1856M-17*, West Conshohocken, PA.

Alkaysi, M., El-Tawil, S., Liu, Z., & Hansen, W. (2016). Effects of silica powder and cement type on durability of ultra high performance concrete (UHPC). *Cement and Concrete Composites*, 66, 47-56.

BSI. (2002). Mixing water for concrete - specification for sampling, testing and assessing the suitability of water, including water recovered from processes in the concrete industry, as mixing water for concrete. *BSI EN 1008*, London, UK.

BSI. (2013). Aggregates for concrete, *BS EN1260*, London, UK.

Carreira, D. J., and Chu, K. H. (1985). Stress-strain relationship for plain concrete in compression. *ACI Journal*, 82(6), 797-804.

CLP, Hong Kong. (2018). https://www.clp.com.hk/zh/customer-service/tariff/business-and-other-customers/bulk-tariff (accessed 20/08/18).

Dickson, A. G., & Goyet, C. (1994) *Handbook of Methods for the Analysis of the Various Parameters of the Carbon Dioxide System in Sea Water. Version 2*, Oak Ridge National Laboratory, Oak Ridge, 10-12.

De Weerdt, K., Justnes, H., & Geiker, M. R. (2014). Changes in the phase assemblage of concrete exposed to sea water. *Cement and Concrete Composites*, 47, 53-63.

Etxeberria, M., Fernandez, J. M., & Limeira, J. (2016). Secondary aggregates and seawater employment for sustainable concrete dyke blocks production: case study. *Construction and Building Materials*, 113, 586-595.

Fernandes, V. A., Purnell, P., Still, G. T., & Thomas, T. H. (2007). The effect of clay content in sands used for cementitious materials in developing countries. *Cement and Concrete Research*, 37(5), 751-758.

GB/T. (2011). Sand for construction. *GB/T 14684-2011*, Beijing, China. (in Chinese).

Ghorab, H. Y., Hilal, M. S., & Kishar, E. A. (1989). Effect of mixing and curing waters on the behaviour of cement pastes and concrete part 1: microstructure of cement pastes. *Cement and Concrete Research*, 19(6), 868-878.

Graybeal, B., & Tanesi, J. (2007). Durability of an ultrahigh-performance concrete. *Journal of Materials in Civil Engineering*, 19(10), 848-854.

Graybeal, B., & Davis, M. (2008). Cylinder or cube: strength testing of 80 to 200 MPa (11.6 to 29 ksi) ultra-high-performance fiber-reinforced concrete. *ACI Materials Journal,* 105(6), 603-609.

Graybeal, B. A. (2011). *Ultra-High Performance Concrete (No. FHWA-HRT-11-038)*. Federal Highway Administration, Washington, DC, USA.

Hamad, B.S. (1995). Investigations of chemical and physical properties of white cement concrete. *Advanced Cement Based Materials*, 2(4), 161-167.

Hasdemir, S., Tuğrul, A., & Yılmaz, M. (2016). The effect of natural sand composition on concrete strength. *Construction and Building Materials*, 112, 940-948.

Hemalatha, T., & Ramaswamy, A. (2017). A review on fly ash characteristics–towards promoting high volume utilization in developing sustainable concrete. *Journal of Cleaner Production*, 147, 546-559.

Hewlett P.C. (1998). *LEA's Chemistry of Cement and Concrete*, John Wiley& Sons Inc., New York, USA.

HK CSD. (2018a). *Average Wholesale Prices of Selected Building Materials in April 2018*, Census and Statistics Department, Hong Kong.

HK CSD. (2018b). *Average Daily Wages of Workers Engaged in Public Sector Construction Projects as Reported by Main Contractors in May 2018*, Census and Statistics Department, Hong Kong.

HK WSD. (2018). https://www.wsd.gov.hk/tc/customer-services/manage-account-and-water-bills/water-sewage-tariff/index.html (accessed 11/01/2019).

Hoang, A. L., & Fehling, E. (2017). Influence of steel fiber content and aspect ratio on the uniaxial tensile and compressive behavior of ultra high performance concrete. *Construction and Building Materials*, 153, 790-806.

Islam, M. M., Islam, M. S., Al-Amin, M., & Islam, M. M. (2012). Suitability of sea water on curing and compressive strength of structural concrete. *Journal of Civil Engineering (IEB),* 40, 37-45.

JGJ. (2006). Mixing water for concrete. *JGJ 63-2006*, Beijing, China. (in Chinese).

JGJ. (2006). Standard for technical requirements and test method of sand and crushed stone (or gravel) for ordinary concrete. *JGJ 52-2006*, Beijing, China. (in Chinese).

JGJ. (2010). Technical code for application of sea-sand concrete. *JGJ206-2010*, Beijing, China. (in Chinese).

Juengera, M. C. G., Monteirob, P. J. M., Gartnerc, E. M. & Denbeauxd, G. P. (2016). A soft X-ray microscope investigation into the effects of calcium chloride on tricalcium silicate hydration. *Cement and Concrete Research*, 35, 19-25.

Kaushik, S. K., & Islam, S. (1995). Suitability of sea water for mixing structural concrete exposed to a marine environment. *Cement and Concrete Composites*, 17(3), 177-185.

Kusumawardaningsih, Y., Fehling, E., & Ismail, M. (2015). UHPC compressive strength test specimens: Cylinder or cube?. *Procedia Engineering*, 125, 1076-1080.

Li, Y. L., Zhao, X. L., Singh, R. R., & Al-Saadi, S. (2016). Tests on seawater and sea sand concrete-filled CFRP, BFRP and stainless steel tubular stub columns. *Thin-Walled Structures*, 108, 163-184.

Li, Y. L., Teng, J. G., Zhao, X. L., & Raman, R. S. (2018). Theoretical model for seawater and sea sand concrete-filled circular FRP tubular stub columns under axial compression. *Engineering Structures*, 160, 71-84.

Liu, W., Cui, H., Dong, Z., Xing, F., Zhang, H., & Lo, T. Y. (2016). Carbonation of concrete made with dredged marine sand and its effect on chloride binding. *Construction and Building Materials*, 120, 1-9.

Lu, Z. H., & Zhao, Y. G. (2010). Empirical stress-strain model for unconfined high-strength concrete under uniaxial compression. *Journal of Materials in Civil Engineering*, 22(11), 1181-1186.

Mewarhitech, India. (2018). http://www.mewarhitech.com/sand-washer-machine/ (accessed 20/08/2018).

Mohammed, T. U., Hamada, H., & Yamaji, T. (2004). Performance of seawater-mixed concrete in the tidal environment. *Cement and Concrete Research*, 34(4), 593-601.

Meng, W. N., & Khayat, K. (2017). Effects of saturated lightweight sand content on key characteristics of ultra-high-performance concrete. *Cement and Concrete Research*, 101, 46-54.

Nishida, T., Otsuki, N., Ohara, H., Garba-Say, Z. M., & Nagata, T. (2013). Some considerations for applicability of seawater as mixing water in concrete. *Journal of Materials in Civil Engineering*, 27(7), B4014004.

Papadakis, V. G. (2000). Effect of fly ash on Portland cement systems: Part II. High-calcium fly ash. *Cement and Concrete Research*, *30*(10), 1647-1654.

Ragab, A. M., Elgammal, M. A., Hodhod, O. A., & Ahmed, T. E. (2016). Evaluation of field concrete deterioration under real conditions of seawater attack. *Construction and Building Materials*, 119, 130-144.

Ramachandran, V.S. (1979). Differential thermal method of estimating calcium hydroxide in calcium silicate and cement pastes, *Cement and Concrete Research*, 9(6), 677-684

Richard, P., & Cheyrezy, M. (1995). Composition of reactive powder concretes. *Cement and Concrete Composites*, 25(7), 1501-1511.

Richardson, A. E., & Fuller, T. (2013). Sea shells used as partial aggregate replacement in concrete. *Structural Survey*, 31(5), 347-354.

Roux, N., Andrade, C., & Sanjuan, M. (1996). Experimental study of durability of reactive powder concretes. *Journal of Materials in Civil Engineering*, 8(1), 1-6.

Sakai, E., Akinori, N., Daimon, M., Aizawa, K., & Kato, H. (2008). Influence of Superplasticizer on the Fluidity of Cements with Different Amount of Aluminate Phase. *Second International Symposium on Ultra High Performance Concrete*, 85-92.

Shi, Z. G., Shui, Z. H., Li, Q., & Geng, H. N. (2015). Combined effect of metakaolin and sea water on performance and microstructures of concrete. *Construction and Building Materials*, 74, 57-64.

Shi, C., Wu, Z., Xiao, J., Wang, D., Huang, Z., & Fang, Z. (2015). A review on ultra high performance concrete: Part I. Raw materials and mixture design. *Construction and Building Materials*, 101, 741-751.

Sobuz, H. R., Visintin, P., Ali, M. M., Singh, M., Griffith, M. C., & Sheikh, A. H. (2016). Manufacturing ultra-high performance concrete utilising conventional materials and production methods. *Construction and Building materials*, 111, 251-261.

Soliman, N. A., & Tagnit-Hamou, A. (2017). Using glass sand as an alternative for quartz sand in UHPC. *Construction and Building Materials*, 145, 243-252.

Suryavanshi, A. K., & Swamy, R. N. (1996). Stability of Friedel's salt in carbonated concrete structural elements. *Cement and Concrete Research*, 26(5), 729-741.

Taylor, M. A., & Kuwairi, A. (1978). Effect of ocean salts on the compressive strength of concrete. *Cement and Concrete Research*, 8, 491-500.

Teng, J. G. (2014). Performance enhancement of structures through the use of fibre-reinforced polymer (FRP) composites, in: *Proceedings of 23rd Australasian Conference on the Mechanics of Structures and Materials (ACMSM23)*, New south wales, Australia.

Teng, J. G., Yu, T., Dai, J. G., & Chen, G. M. (2011). FRP composites in new construction: current status and opportunities, in: *Proceedings of 7th National Conference on FRP Composites in Infrastructure*, Hangzhou, China.

Teng, J.G., Zhang, B., Zhang, S.S. & Fu, B. (2018). Steel-free hybrid reinforcing bars for concretes structures. *Advances in Structural Engineering*, 21(16), 2617-2621.

Tikalsky, P.J., & Carrasquillo, R. L. (1989) *The Effect of Fly Ash on the Sulfate Resistance of Concrete. Research Report 481-5*, Center for Transportation Research, the University of Texas at Austin, 15-16.

Tiwari, P., Chandak, R., & Yadav, R. K. (2014). Effect of salt water on compressive strength of concrete. *International Journal of Engineering Research and Applications*, 4(4), 38-42.

Wang, J., Feng, P., Hao, T., & Yue, Q. (2017). Axial compressive behaviour of seawater coral aggregate concrete-filled FRP tubes. *Construction and Building Materials*, 147, 272-285.

Wegian, F. M. (2010). Effect of seawater for mixing and curing on structural concrete. *The IES Journal Part A: Civil & Structural Engineering*, 3(4), 235-243.

Whipmix, USA, (2019). https://whipmix.com/products/silky-rock/ (accessed 11.01.2019).

Wille, K., Naaman, A. E., & Parra-Montesinos, G. J. (2011). Ultra-high-performance concrete with compressive strength exceeding 150 MPa (22 ksi): A Simpler Way. *ACI Materials Journal,* 108(1), 46-54.

Wille, K., El-Tawil, S., & Naaman, A. E. (2014). Properties of strain hardening ultra high performance fiber reinforced concrete (UHP-FRC) under direct tensile loading. *Cement and Concrete Composites*, 48, 53-66.

Wille, K., & Boisvert-Cotulio, C. (2015). Material efficiency in the design of ultra-high-performance concrete. *Construction and Building Materials,* 86, 33-43.

Wu, Z., Shi, C., He, W., & Wang, D. (2016). Uniaxial compression behavior of ultra-high performance concrete with hybrid steel fiber. *Journal of Materials in Civil Engineering*, *28*(12), 06016017.

Xiao, J., Qiang, C., Nanni, A., & Zhang, K. (2017). Use of sea-sand and seawater in concrete construction: current status and future opportunities. *Construction and Building Materials*, 155, 1101-1111.

Yang, E. I., Yi, S.T., & Leem, Y.M. (2005). Effect of oyster shell substituted for fine aggregate on concrete characteristics: Part I. Fundamental properties, *Cement and Concrete Research*. 35 (11), 2175-2182.

Younis, A., Ebead, U., Suraneni, P., & Nanni, A. (2018). Fresh and hardened properties of seawater-mixed concrete. *Construction and Building Materials*, 190, 276-286.

Zhang, B., Yu, T., & Teng, J. G. (2014). Behavior of concrete-filled FRP tubes under cyclic axial compression. *Journal of Composites for Construction*, 19(3), 04014060.

Figures

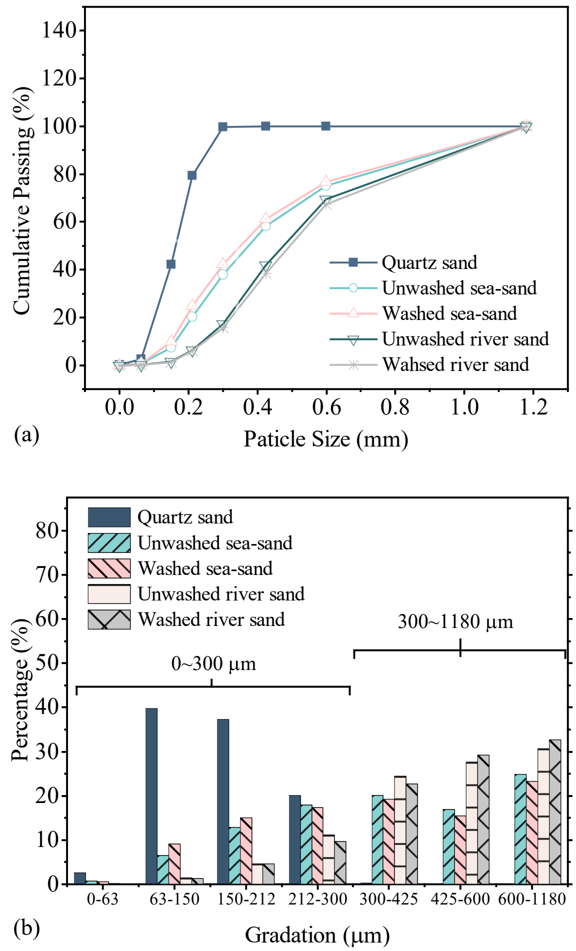

Figure 1. Particle size distributions of sands: (a) cumulative passing; and (b) gradations.

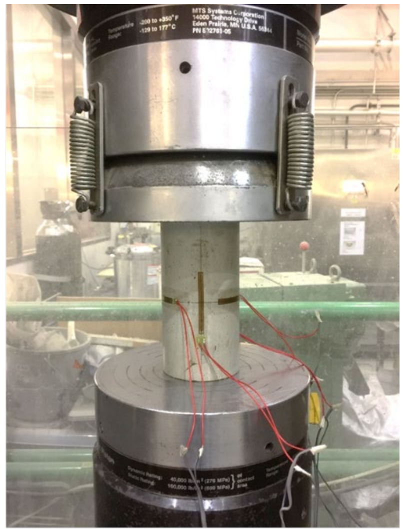

(a)

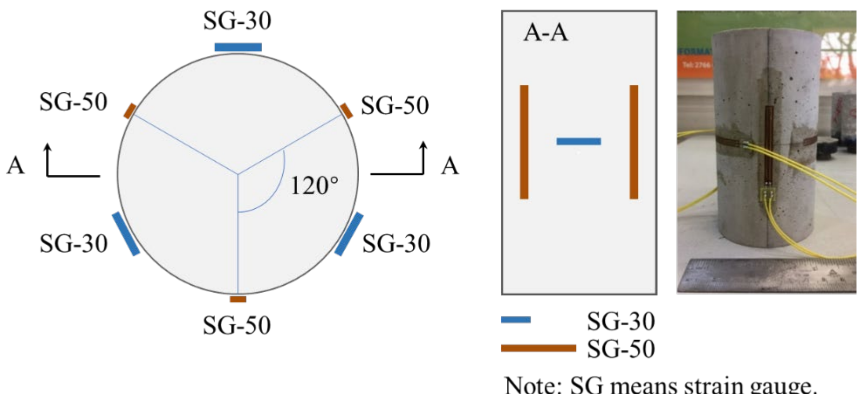

(b)

Figure 2. Test setup and instrumentation: (a) test setup; (b) layout of strain gauges.

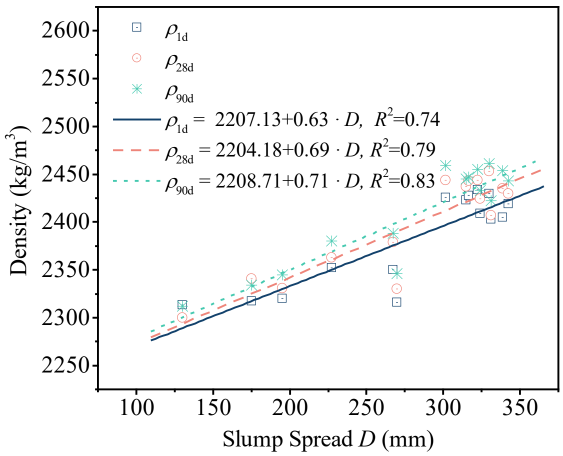

Figure 3. Relationship between density and slump spread.

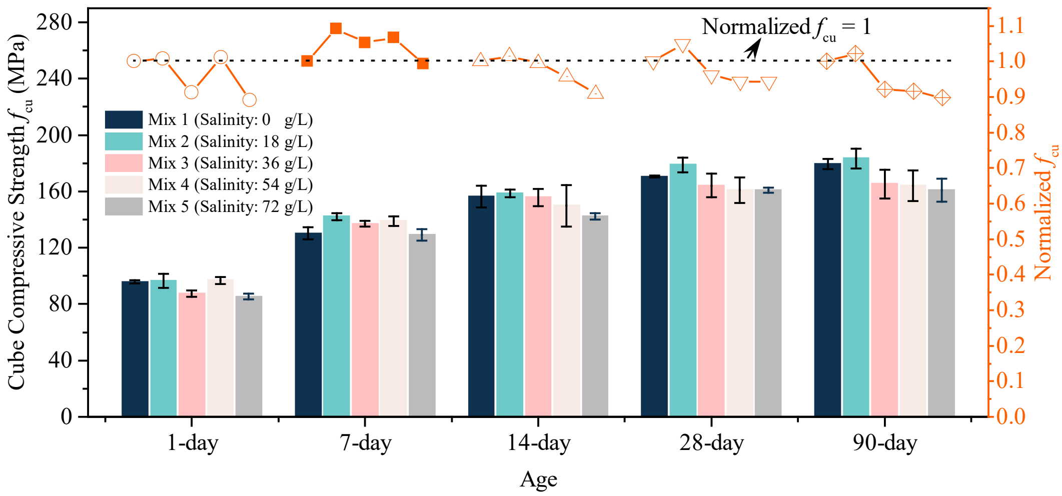

Figure 4. Effect of salinity on compressive strength.

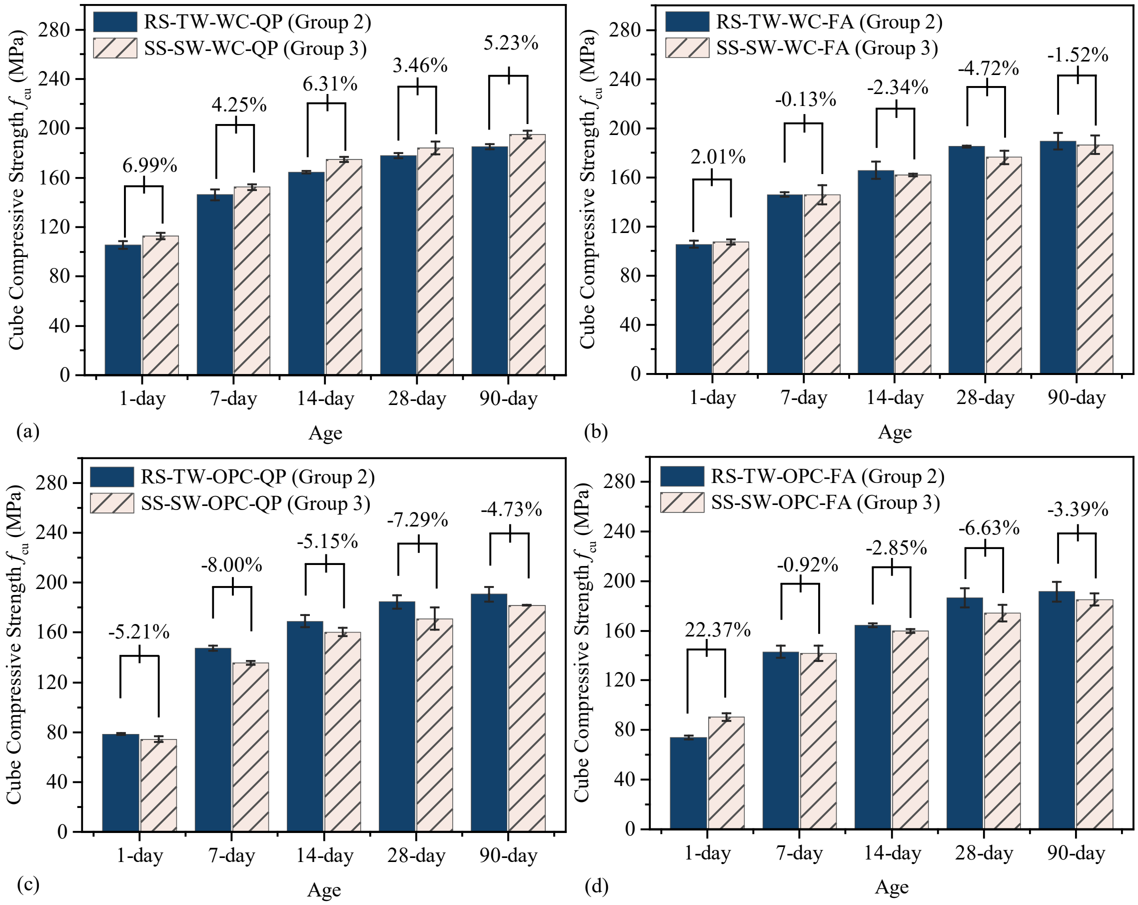

Figure 5. Effect of seawater and sea-sand on the strength development of UHPC prepared with: (a) white cement and quartz powder; (b) white cement and fly ash; (c) ordinary Portland cement and quartz powder; and (d) ordinary Portland cement and fly ash.

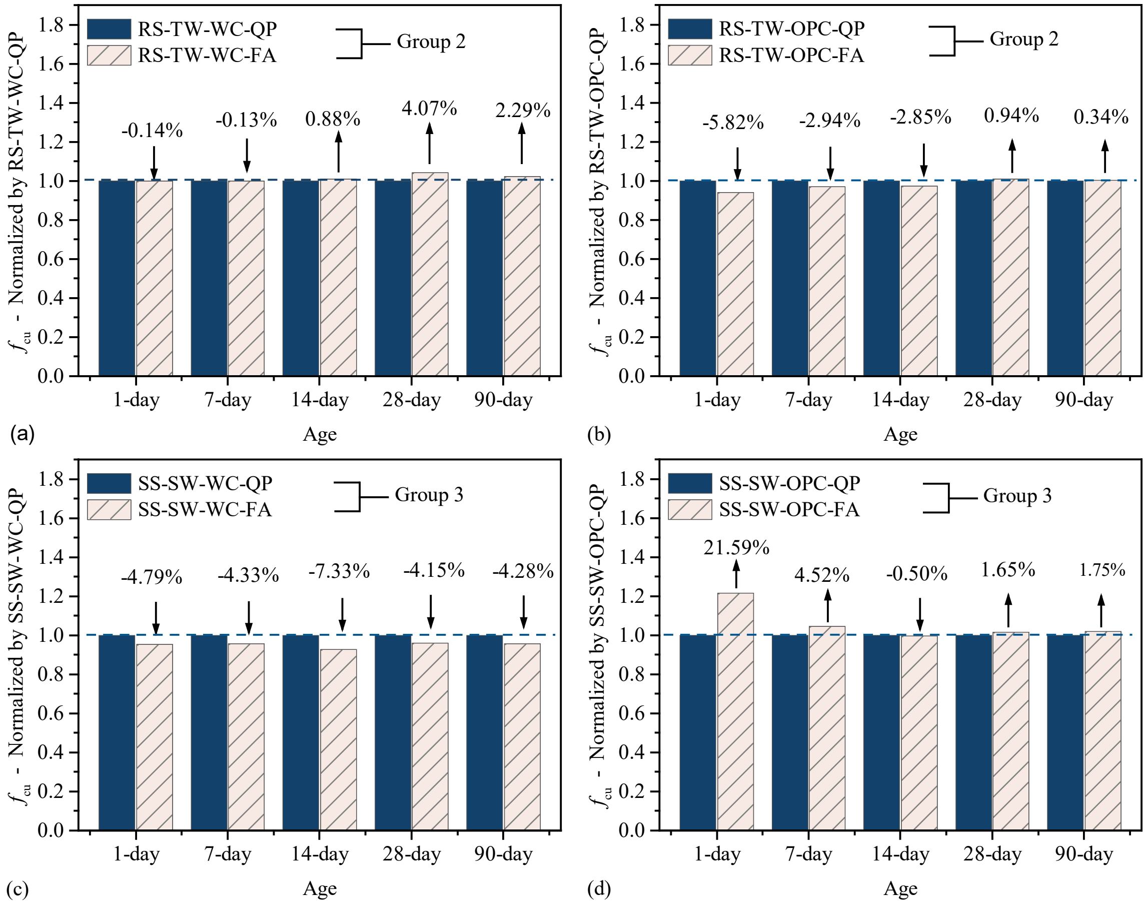

Figure 6. Effect of supplementary material type on strength development: (a) tap water-river sand UHPC with white cement; (b) tap water-river sand UHPC with ordinary Portland cement; (c) UHPSSC with white cement; and (d) UHPSSC with ordinary Portland cement.

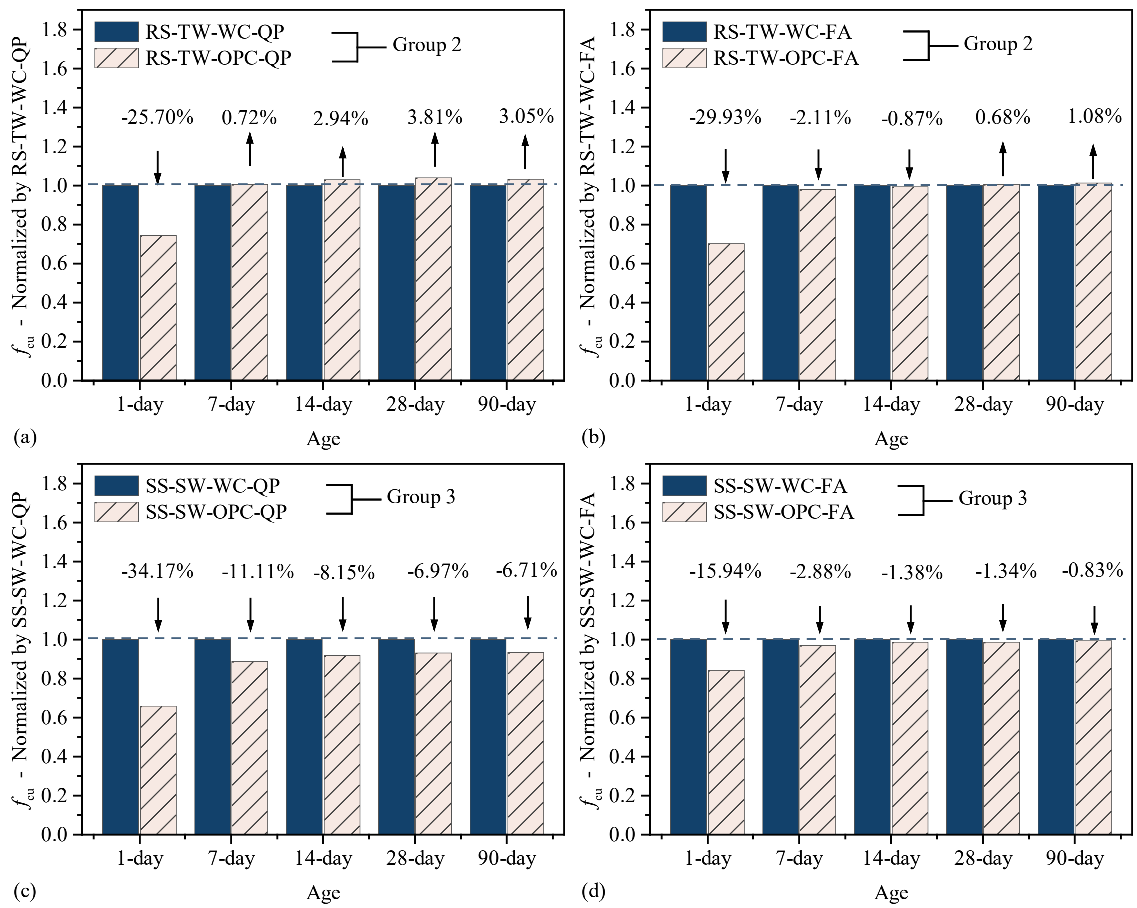

Figure 7. Effect of cement type on strength development: (a) tap water-river sand UHPC with quartz powder; (b) tap water-river sand UHPC with fly ash; (c) UHPSSC with quartz powder; and (d) UHPSSC with fly ash.

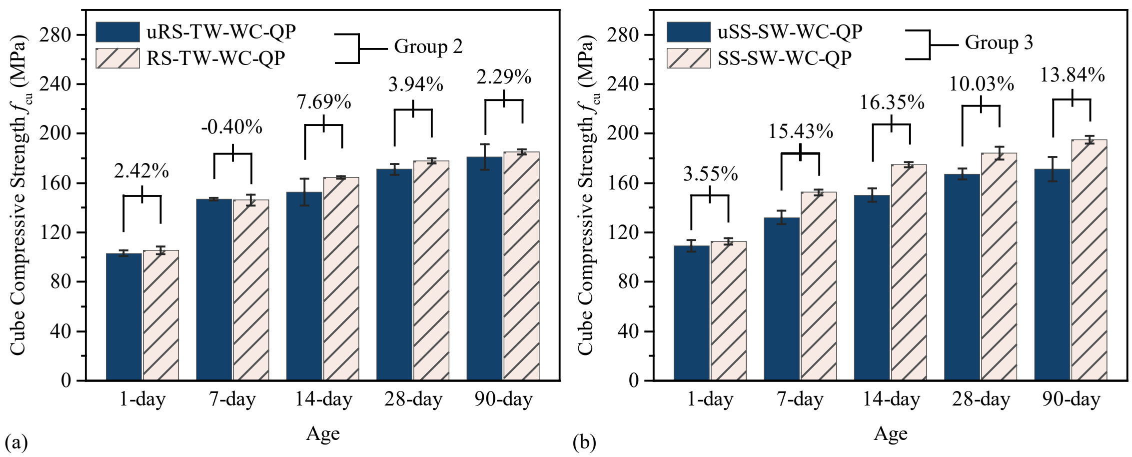

Figure 8. Effect of sand desilting on strength development: (a) tap water-river sand UHPC; and (b) UHPSSC.

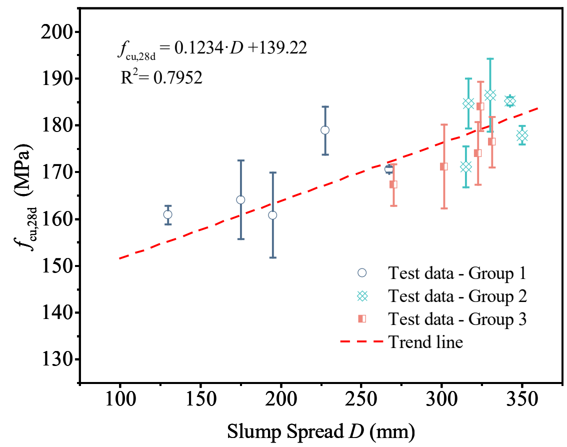

Figure 9. Relationship between 28-day cube compressive strength and slump spread.

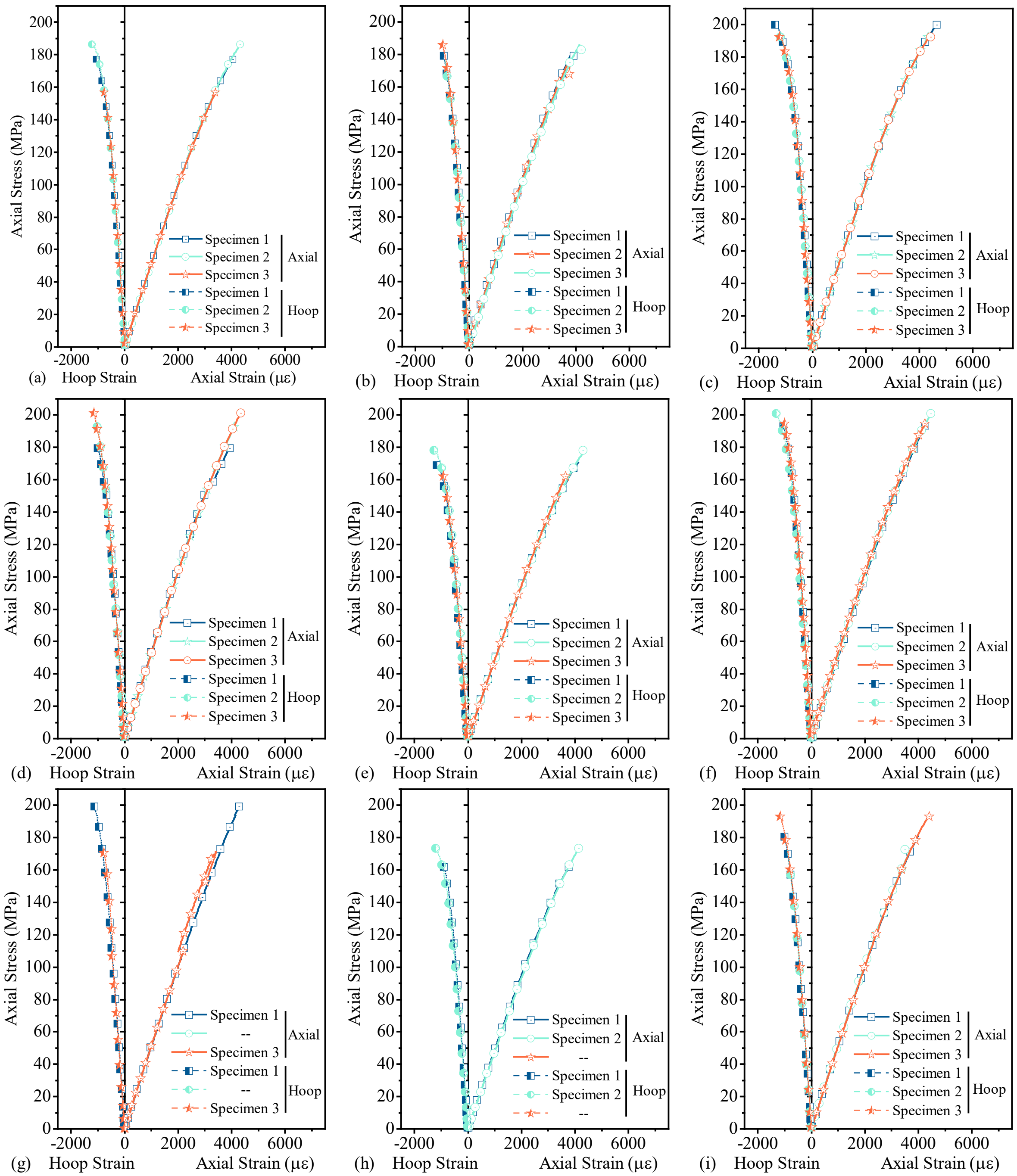

Figure 10. Stress-strain curves:
(a) uRS-TW-WC-QP; (b) RS-TW-WC-QP; (c) RS-TW-OPC-QP; (d) RS-TW-OPC-FA; (e) uSS-SW-WC-QP; (f) SS-SW-WC-QP; (g) SS-SW-WC-FA; (h) SS-SW-OPC-QP; (i) SS-SW-OPC-FA.

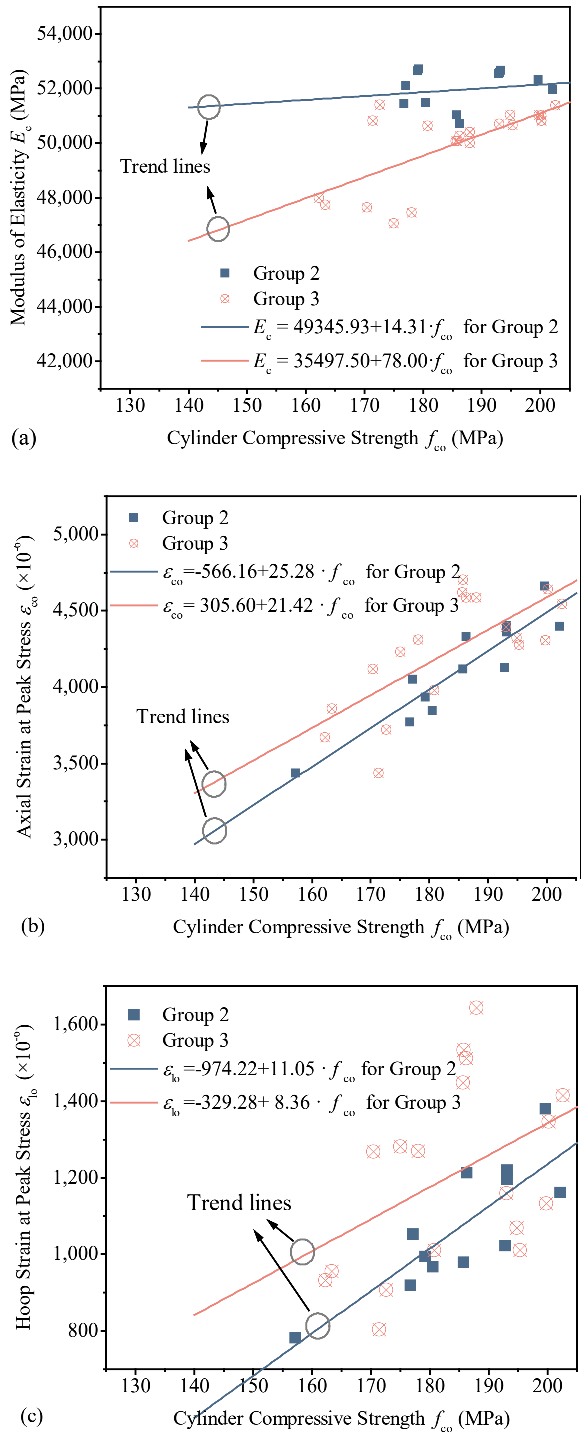

Figure 11. Characteristic parameters versus cylinder compressive strength: (a) E_c; (b) ε_{co}; and (c) ε_{lo}.

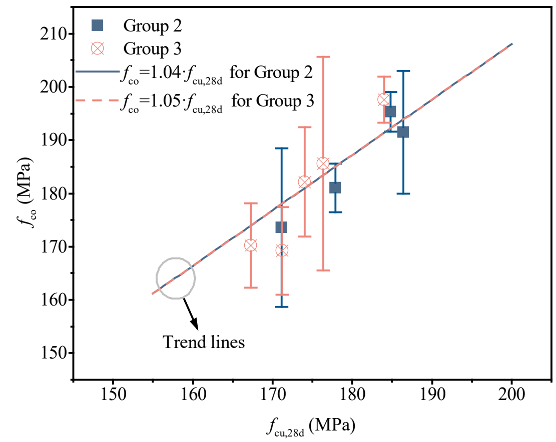

Figure 12. Relationship between cylinder compressive strength (f_{co}) and 28-day cube compressive strength ($f_{cu,28d}$).

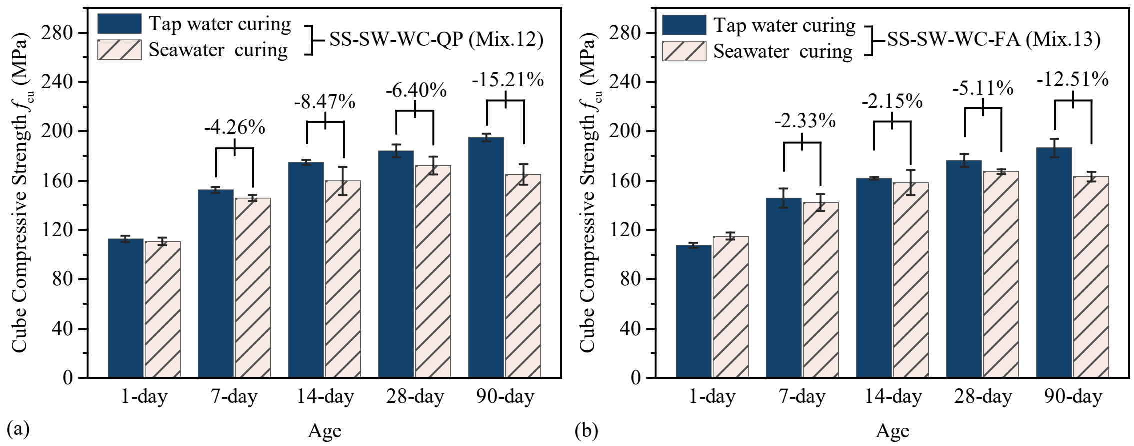

Figure 13. Effect of seawater curing on the strength development of UHPSSC.

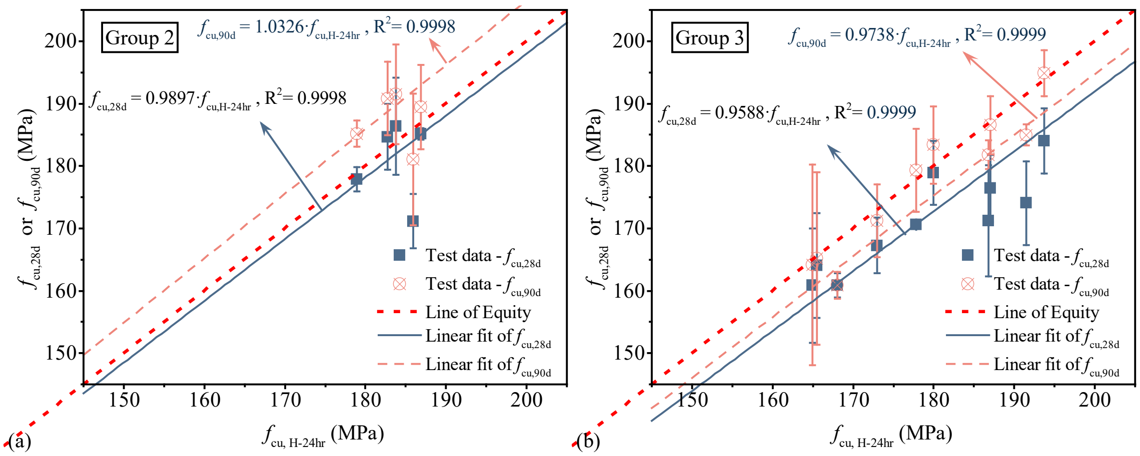

Figure 14. 28 and 90-day tap water immersion-cured cube compressive strengths (i.e. $f_{cu,28d}$ and $f_{cu,90d}$) versus 24-hour heat-cured cube compressive strengths (i.e. $f_{cu,H-24hr}$): (a) Group 2 (tap water-river sand UHPC); (b) Group 3 (UHPSSC).

Tables

Table 1. Mix proportions (in kg/m^3)

Group number	Mix Number	Mix name	Cement		SF	SM		Fine aggregate					Water						HRWR
			WC	OPC		QP	FA	QS	uRS	RS	uSS	SS	TW	50AW	100AW	150AW	200AW	SW	
	1	QS-TW-WC-QP	830		207	207		913					164						27
	2	QS-50ASW-WC-QP	830		207	207		913						164					27
1	3	QS-100ASW-WC-QP	830		207	207		913							164				27
	4	QS-150ASW-WC-QP	830		207	207		913								164			27
	5	QS-200ASW-WC-QP	830		207	207		913									164		27
	6	uRS-TW-WC-QP	830		207	207			913				164						27
	7	RS-TW-WC-QP	830		207	207				913			164						27
2	8	RS-TW-WC-FA	830		207		207			913			164						27
	9	RS-TW-OPC-QP		830	207	207				913			164						27
	10	RS-TW-OPC-FA		830	207		207			913			164						27
	11	uSS-SW-WC-QP	830		207	207					913							164	27
	12	SS-SW-WC-QP	830		207	207						913						164	27
3	13	SS-SW-WC-FA	830		207		207					913						164	27
	14	SS-SW-OPC-QP		830	207	207						913						164	27
	15	SS-SW-OPC-FA		830	207	207						913						164	27

Note: WC - white cement; OPC - ordinary Portland cement; SF - silica fume; SM - supplemental material; QP - quartz powder; FA - Class C fly ash; QS - quartz sand; uRS - unwashed river sand; RS - river sand; uSS - unwashed sea-sand; SS - sea-sand; TW - tap water; 50ASW - artificial seawater whose salinity is half that of typical natural seawater (TNSW); 100ASW - artificial seawater whose salinity is the same as that of TNSW; 150ASW - artificial seawater whose salinity is 1.5 times that of TNSW; 200ASW - artificial seawater whose salinity is twice that of TNSW; SW - natural seawater; HRWR - high range water reducer.

Table 2. Chemical and phase compositions of cements, silica fume and supplemental materials

Item	Identification	WC	OPC	SF	QP	FA
Chemical composition (in %)	SiO_2	21.60	20.00	94.20	96.40	29.90
	Fe_2O_3	0.41	3.04	0.35	0.14	16.00
	Al_2O_3	5.16	5.53	0.71	0.74	16.20
	CaO	65.55	64.30	0.13	0.81	18.90
	TiO_2	0.17	0.23	--	--	0.74
	SO_3	3.63	4.49	0.17	0.90	3.99
	MgO	2.40	1.28	--	0.10	6.74
	Na_2O	--	--	--	--	4.89
	K_2O	0.26	0.62	0.09	--	1.48
	ZnO	--	0.02	--	--	0.03
	ZrO_2	--	--	3.84	--	--
Bogue components (in %)	C_3S	57.00	55.40	--	--	--
	C_2S	19.02	15.63	--	--	--
	C_3A	12.99	9.52	--	--	--
	C_4AF	1.24	9.24	--	--	--

Table 3. Chemical compositions of natural seawater, artificial seawater and tap water (in g/L)

Ion	Seawater average (Dickson and Goyet 1994)	Tap water	Natural seawater			Artificial seawater		
			Chek Lap Kok	Whampoa	Repulse Bay	Salt 1	Salt 2	Salt 3
F^-	0.0013	0.0005	0.0000	0.0001	0.0000	0.0000	0.0000	0.0000
Cl^-	19.3524	0.0116	18.1526	19.0211	18.3124	17.7812	21.1087	19.8642
Br^-	0.0673	0.0000	0.0659	0.0991	0.0738	0.0617	0.0000	0.0000
SO_4^{2-}	2.7123	0.0176	1.6750	2.7282	1.6998	1.7438	0.0326	0.2045
NO_2^-	--	0.0000	0.0000	0.0000	0.0649	0.0000	0.0000	0.0000
NO_3^-	--	0.0099	0.0000	0.0138	0.0314	0.0285	0.0000	0.0283
PO_4^{3-}	--	0.0000	0.0000	0.0000	0.0000	0.0000	0.0000	0.0000
Li^+	--	0.0000	0.0007	0.0006	0.0006	0.0006	0.0005	0.0005
Na^+	10.7837	0.0091	10.4194	11.2169	11.1388	11.0738	15.0646	13.6546
NH_4^+	--	0.0000	0.0000	0.0148	0.0179	0.0057	0.0289	0.0000
K^+	0.3991	0.0035	0.3544	0.3923	0.3926	0.4329	0.0432	0.1526
Mg^{2+}	1.2837	0.0018	1.2152	1.3497	1.3410	1.2913	0.0135	0.3439
Ca^{2+}	0.4121	0.0169	0.3582	0.4060	0.4535	0.4609	0.0422	0.0789
Salinity	35.0119	0.0709	32.2413	35.2428	33.5268	32.8803	36.3342	34.3275

Table 4. Chemical compositions of sand lixiviums (in g/L)

Ion	Tap water	Natural seawater	Lixivium			
		Chek Lap Kok	River sand (Untreated)	Sea-sand (Untreated)	Sea-sand (Washed by tap water)	Sea-sand (Washed by tap water and soaked by seawater)
F^-	0.0005	0.0000	0.0000	0.0000	0.0000	0.0000
Cl^-	0.0116	18.1526	0.0119	1.8554	0.0130	1.9200
Br^-	0.0000	0.0659	0.0000	0.0000	0.0000	0.0780
SO_4^{2-}	0.0176	1.6750	0.1235	0.1817	0.0119	0.2134
NO_2^-	0.0000	0.0000	0.0000	0.0000	0.0000	0.0169
NO_3^-	0.0099	0.0000	0.0000	0.0000	0.0000	0.0000
PO_4^{3-}	0.0000	0.0000	0.0000	0.0000	0.0000	0.0000
Li^+	0.0000	0.0007	0.0000	0.0000	0.0000	0.0000
Na^+	0.0091	10.4194	0.0456	2.2585	0.0238	1.1284
NH_4^+	0.0000	0.0000	0.0000	0.0000	0.0000	0.0000
K^+	0.0035	0.3544	0.0101	0.0884	0.0074	0.0480
Mg^{2+}	0.0018	1.2152	0.0190	0.1857	0.0056	0.0612
Ca^{2+}	0.0169	0.3582	0.1478	0.1112	0.0603	0.4575
Salinity	0.0709	32.2413	0.3579	4.6809	0.1221	3.9233

Table 5. Workability and densities of all mixes

Group number	Mix number	Mix name	Slump spread (mm)	ρ_{1d} (kg/m^3)	ρ_{28d} (kg/m^3)	ρ_{90d} (kg/m^3)
1	1	QS-TW-WC-QP	267.50	2350	2379	2388
	2	QS-50ASW-WC-QP	227.50	2352	2363	2380
	3	QS-100ASW-WC-QP	175.00	2317	2341	2334
	4	QS-150ASW-WC-QP	195.00	2320	2331	2345
	5	QS-200ASW-WC-QP	130.00	2313	2300	2312
2	6	uRS-TW-WC-QP	315.00	2423	2437	2445
	7	RS-TW-WC-QP	338.75	2405	2435	2454
	8	RS-TW-WC-FA	342.50	2419	2430	2443
	9	RS-TW-OPC-QP	316.67	2428	2443	2447
	10	RS-TW-OPC-FA	330.00	2430	2453	2461
3	11	uSS-SW-WC-QP	270.00	2316	2330	2346
	12	SS-SW-WC-QP	324.17	2409	2424	2433
	13	SS-SW-WC-FA	331.25	2403	2407	2422
	14	SS-SW-OPC-QP	301.67	2426	2444	2459
	15	SS-SW-OPC-FA	322.50	2434	2444	2455

Table 6. Cube compressive strengths of all mixes

Group number	Mix number	Mix name	$f_{cu,1d}$ (MPa)		$f_{cu,7d}$ (MPa)		$f_{cu,14d}$ (MPa)		$f_{cu,28d}$ (MPa)		$f_{cu,90d}$ (MPa)		$f_{cu,H\text{-}24hr}$ (MPa)	
			Mean	SD	Mean	SD	Mean	SD	Mean	SD	Mean	SD	Mean	SD
1	1	QS-TW-WC-QP	95.80	1.07	130.13	4.30	156.48	7.71	170.57	0.59	179.28	3.56	177.83	6.66
	2	QS-50ASW-WC-QP	96.60	4.88	142.07	2.70	158.77	2.70	178.90	5.13	183.35	7.15	179.94	6.20
	3	QS-100ASW-WC-QP	87.38	2.30	137.04	1.86	155.72	6.10	164.07	8.42	165.19	10.26	165.53	13.82
	4	QS-150ASW-WC-QP	96.85	2.42	138.95	3.29	149.87	14.75	160.83	9.13	164.15	10.79	164.96	16.06
	5	QS-200ASW-WC-QP	85.31	2.00	129.27	4.04	142.28	2.32	160.84	1.93	160.91	8.22	168.06	2.15
2	6	uRS-TW-WC-QP	103.11	2.48	146.84	0.92	152.60	10.88	171.15	4.38	181.03	10.54	185.92	5.03
	7	RS-TW-WC-QP	105.60	2.93	146.26	4.38	164.33	0.96	177.89	1.93	185.18	2.13	178.91	22.05
	8	RS-TW-WC-FA	105.45	2.87	146.06	1.91	165.78	7.16	185.14	0.91	189.42	6.76	186.85	0.42
	9	RS-TW-OPC-QP	78.46	0.70	147.31	1.92	169.17	4.85	184.66	5.28	190.82	5.86	182.72	2.95
	10	RS-TW-OPC-FA	73.89	1.50	142.98	4.83	164.34	1.46	186.40	7.79	191.47	8.02	183.78	20.84
3	11	uSS-SW-WC-QP	109.10	4.69	132.09	5.44	150.16	5.39	167.27	4.42	171.17	9.87	173.00	5.83
	12	SS-SW-WC-QP	112.98	2.62	152.47	2.25	174.71	1.97	184.04	5.21	194.86	2.99	193.71	3.67
	13	SS-SW-WC-FA	107.57	2.20	145.86	7.58	161.90	0.96	176.41	5.39	186.53	7.69	187.01	4.64
	14	SS-SW-OPC-QP	74.37	2.34	135.53	1.63	160.46	3.20	171.21	8.92	181.80	0.31	186.83	2.33
	15	SS-SW-OPC-FA	90.42	3.21	141.66	6.13	159.66	1.43	174.03	6.71	184.98	4.91	191.48	1.70

Table 7. Characteristic parameters of stress-strain curve

Group number	Mix number	Mix name	f_{co} (MPa)		E_c (GPa)		υ		ε_{co} ($\times 10^{-6}$)		ε_{lo} ($\times 10^{-6}$)	
			Mean	SD	Mean	SD	Mean	SD	Mean	SD	Mean	SD
2	6	uRS-TW-WC-QP	173.54	14.88	51.542	0.745	0.20	0.00	3938	458	1015	218
	7	RS-TW-WC-QP	181.00	4.53	51.315	0.257	0.20	0.00	3912	184	955	32
	9	RS-TW-OPC-QP	195.34	3.74	52.509	0.180	0.21	0.00	4473	163	1264	100
	10	RS-TW-OPC-FA	191.44	11.51	52.403	0.385	0.21	0.00	4150	233	1059	89
3	11	uSS-SW-WC-QP	170.25	7.92	47.690	0.279	0.21	0.00	4032	329	1156	195
	12	SS-SW-WC-QP	197.59	4.35	51.024	0.362	0.20	0.01	4381	144	1165	219
	13	SS-SW-WC-FA	185.57	20.03	50.924	0.141	0.21	0.01	3870	614	968	232
	14	SS-SW-OPC-QP	169.21	8.23	47.388	0.489	0.21	0.01	4044	264	1118	231
	15	SS-SW-OPC-FA	182.16	10.27	50.910	0.431	0.22	0.00	4031	340	1026	126

Table 8. Effects of curing methods on properties of UHPSSC

Mix name	SS-SW-WC-QP (Mix 12/Group 3)		SS-SW-WC-FA (Mix 13/Group 3)	
Curing method	Tap water curing	Seawater curing	Tap water curing	Seawater curing
ρ_{1d} (kg/m^3)	2405	2409	2419	2403
ρ_{28d} (kg/m^3)	2435	2433	2430	2449
ρ_{90d} (kg/m^3)	2454	2446	2443	2446
$f_{cu,1d}$ (MPa)	112.98	110.91	107.57	115.01
$f_{cu, 7d}$ (MPa)	152.47	145.98	145.86	142.47
$f_{cu, 14d}$ (MPa)	174.71	159.91	161.9	158.43
$f_{cu, 28d}$ (MPa)	184.04	172.26	176.41	167.39
$f_{cu, 90d}$ (MPa)	194.86	165.22	186.53	163.19
f_{co} (MPa)	197.59	185.57	185.87	194.10
E_c (GPa)	51.024	50.924	50.132	50.499
υ	0.20	0.21	0.21	0.21
ε_{co} ($\times 10^{-6}$)	4381	3870	4636	4613
ε_{lo} ($\times 10^{-6}$)	1165	968	1497	1495

Table 9. Cost Comparison

Group number	Mix number	Mix name	$f_{cu,28d}$ (MPa)	Cost (HKD/m^3)	Cost per MPa (HKD/MPa/m^3)
--	--	Normal concrete	54.1	587	10.84
3	11	uSS-SW-WC-QP	167	3109 (2982)	18.59 (17.83)
	12	SS-SW-WC-QP	184	3109 (2982)	16.89 (16.20)
	13	SS-SW-WC-FA	176	2695 (2568)	15.28 (14.56)
	14	SS-SW-OPC-QP	171	2055 (1928)	12.02 (11.27)
	15	SS-SW-OPC-FA	174	1641 (1514)	9.43 (8.70)